INSTITUTE OF PHYSICS PUBLISHING CLASSICAL AND QUANTUM GRAVITY

Class. Quantum Grav. **22** (2005) S891–S900 doi:10.1088/0264-9381/22/18/S03

Preparing GEO 600 for gravitational wave astronomy—a status report

M Hewitson (for the LIGO Scientific Collaboration)

Max-Planck-Institut für Gravitationsphysik (Albert-Einstein-Institut) und Universität Hannover, Callinstr. 38, D-30167 Hannover, Germany

E-mail: martin.hewitson@aei.mpg.de

Received 24 March 2005, in final form 15 May 2005
Published 23 August 2005
Online at stacks.iop.org/CQG/22/S891

Abstract

A number of gravitational wave detectors throughout the world are currently moving from the final stages of commissioning to a more continuous observational mode. Together, these detectors form a global network which will search for gravitational waves from various astrophysical sources, such as continuous wave signals from rotating neutron stars, transient signals from, for example, inspiralling compact objects and supernovae explosions, and stochastic gravitational wave signals from the early universe. GEO 600 is a long baseline laser-interferometric gravitational wave detector which employs advanced optical and suspension techniques to reach its design sensitivity. Almost all of the major installation work at GEO 600 is already completed and the detector is currently being commissioned to prepare it for extended observation periods. The commissioning process involves many activities in the areas of noise reduction, calibration, operational stability and characterization. This report highlights some of the major commissioning steps that have contributed to the increase in sensitivity of the instrument over the period from December 2003 to December 2004. In addition, recent extensions to the on-line calibration scheme used in GEO 600 are briefly discussed.

PACS numbers: 04.80.Nn, 95.55.Ym, 95.75.Kk

1. Introduction

A global network of gravitational wave (GW) detectors is at the final stages of commissioning. The network includes a number of laser-interferometric detectors: 3 detectors from the LIGO project [1] in the USA (2 with 4 km arm-length, 1 with 2 km arm-length); 1 detector from the French–Italian VIRGO project [2] with a 3 km arm-length; a 300 m arm-length detector from the TAMA project [3] in Japan; and a 600 m arm-length detector from the German–British project, GEO 600 [4]. In addition, a number of resonant-mass bar detectors are currently

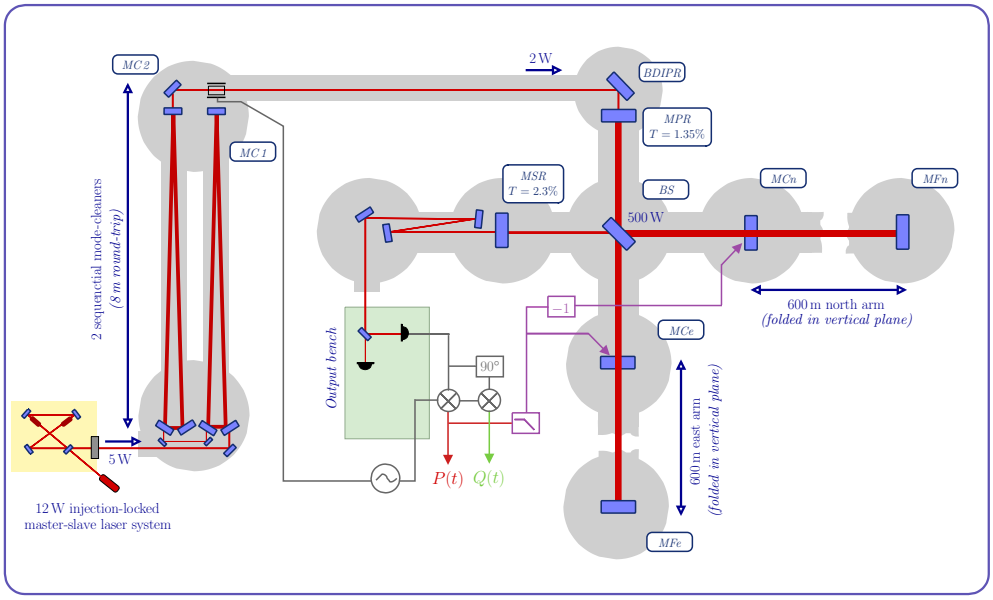

Figure 1. A schematic of the optical layout of GEO 600. Five watts of laser light from a 12 W master/slave laser system is injected into the vacuum system where it is spatially filtered by two sequential mode-cleaners before being injected into the main dual-recycled interferometer. The figure includes a highly simplified sketch of some of the components of the differential-length-control servo used to keep the Michelson at its operating point.

running, for example, the ALLEGRO project [5] in the USA, the AURIGA and Nautilus projects [6, 7] in Italy and the Explorer [7] detector located at CERN. The GEO 600 detector is a Michelson interferometer which uses both power- and signal-recycling to enhance its strain sensitivity; this is known as dual-recycling (see [8, 9] for details). The light source is a 12 W Nd:YAG injection-locked master-slave system [10]. Two sequential mode-cleaners [11] are used to spatially filter the beam before it is injected into the interferometer. The output of the laser was, until recently, attenuated to 3 W before being injected into the vacuum system; this was mainly done to ease locking the interferometer while we are not shot-noise limited at the main detector output photodiode. The injected power in to the mode-cleaners has now been increased to around 5 W. The effect of this power increase is discussed later in this paper in the context of noise hunting and commissioning.

Figure 1 shows a schematic of the optical layout of GEO 600. All of the main optics in GEO 600 are suspended as either double or triple pendulums [12]; the main mirrors of the Michelson interferometer (MCe, MCn, MFe, MFn and BS) are suspended as triple pendulums with monolithic bottom stages [13]. All pendulums are suspended from an upper structure via two wires hung from spring blades. The upper structure is mounted on three stacks that provide a degree of horizontal and vertical isolation from the ground. GEO has four suspended cavities: the two mode-cleaner ring cavities, the power-recycling cavity and the signal-recycling cavity. Each of these cavities has to have both its alignment and length controlled in order to keep the detector at its operating point. A combination of digital and analogue control loops using various actuators is used to achieve this.

Due to the dual-recycled optical configuration of GEO 600, the main GW output signal is spread between two orthogonal demodulated outputs with a frequency-dependent weighting.

This has consequences for the calibration of the instrument (see section 3). For the first half of 2004, only one of the output quadratures (P) was continuously calibrated to apparent strain. Consequently, only this calibrated signal was used to mark the progress of the commissioning work. For the last few months of 2004, the other quadrature (Q) was properly calibrated, providing another measure of progress. Throughout the whole of 2004, the detector was tuned to have a peak response at approximately 1 kHz (by fixing the microscopic length of the signal-recycling cavity).

For the past year (2004), GEO 600 has left the construction phase and moved into an intense period of commissioning during which time no major installation work was carried out. Instead, all effort was focused on noise reduction, debugging of subsystems, calibration, stability improvement, and detector and data characterization. This paper summarizes some of the key steps of the commissioning work of 2004 that have improved the sensitivity of GEO 600 by more than two orders of magnitude at some frequencies, and have brought GEO 600 ever closer to its design sensitivity (see figure 2), preparing it for a long period of gravitational wave observation as part of the global network.

2. Noise hunting and sensitivity improvements

The second half of 2003 saw the installation of the signal-recycling mirror and the development of the control and locking scheme for the dual-recycled interferometer. GEO 600 then entered an extended science run (termed S3 [14]) together with the LIGO detectors and TAMA; only a very short period of time prior to the science run was available for optimizing the new configuration. At the start of 2004, work began to focus strongly on commissioning the dual-recycled interferometer with the main aim to reduce the noise and thus increase the sensitivity of the instrument.

Figure 3 shows the progress of the strain sensitivity of GEO 600 over the period from August 2002 to the end of 2004. The curves are produced by calibrating only the P output quadrature of the detector.

2.1. Major commissioning steps

As well as the many small improvements that were gained during this commissioning period, a few large steps were taken that showed significant sensitivity improvements.

The first of these was the switch of the in-loop control signal for the Michelson Interferometer from that generated by the quadrant diode used for acquisition to the single-element high power diode which provided a signal with lower dark noise (the output noise of the photodiode with no light falling on it). After acquisition, and when the detector is tuned down to its final operating point, the differential-length-control servo switches over to getting its error-point signal from the high-power diode. With the high-power diode in-loop, we are no longer limited in sensitivity by the relatively high dark noise of the quadrant photodetector that is used for acquisition. This step takes us from the curve labelled 'S3 II' in figure 3 to that labelled 'June 2004'.

Following this large improvement, the next major commissioning step was the upgrade of the Michelson differential-length-control servo electronics. A new servo was designed to better account for the signal levels and gain distribution needed to ensure that the entire loop is front-end limited (by dark- and shot-noise of high-power photodiode). Improvement afforded by this new servo system can be seen in the curve labelled 'Sept 2004'.

With this large reduction in low-frequency ($\sim$100 Hz) noise, the sensitivity was at this time limited by coupling of the feedback noise in the signal-recycling longitudinal control

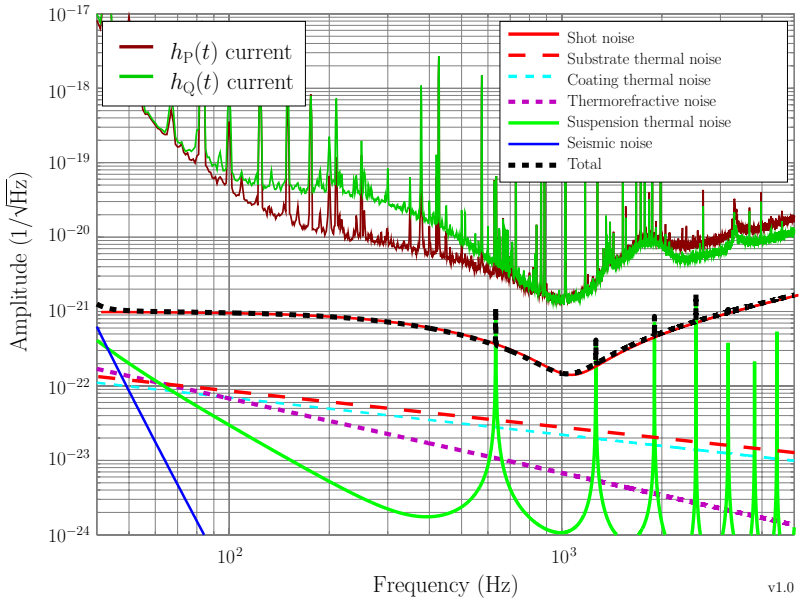

Figure 2. The theoretical sensitivity of GEO 600 in its final optical configuration for a 1 kHz signal-recycling tuning overlaid with the current apparent strain noise of the detector. Almost all of the large lines present in the spectra are injected calibration lines.

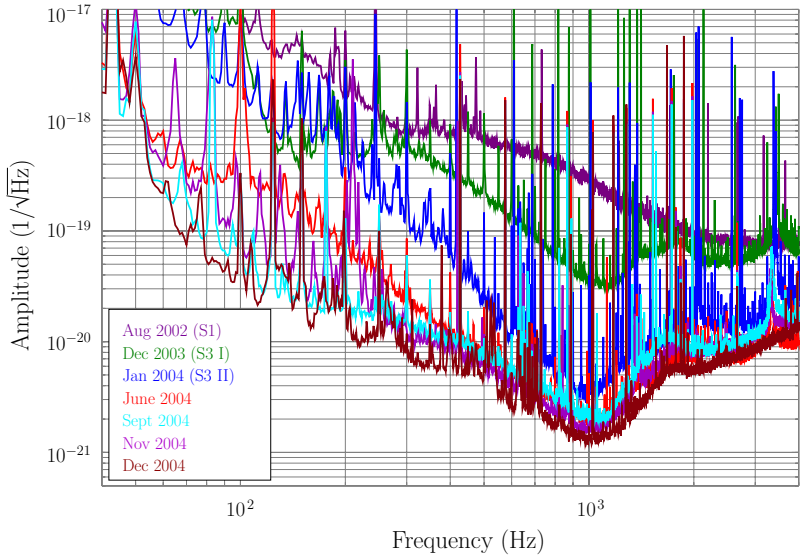

Figure 3. The sensitivity of GEO 600 at various epochs between August 2002 and December 2004. The major increases in sensitivity are discussed in the text. The sensitivity of the power-recycled configuration (S1) is included for reference.

servo to the Michelson differential output. Some logic and switching was added to this servo to allow for switching to a low gain state after the final operating state is reached. This change

gives increased sensitivity in the region from about 80 Hz to 200 Hz. This is indicated in figure 3 by the label 'Nov 2004'.

The final major improvement of 2004 was the discovery of a source of scattered light originating from the optical bench that hosts the photodiode which is used to sense the control modulation sidebands for the signal-recycling length control. The beam that falls on this photodiode comes from the anti-reflective coating of the beam-splitter. This means that any light that is scattered on this optical bench can be directed back into the interferometer and thus can cause a parasitic cavity which, since it is only in the East arm of the Michelson, appears as excess apparent differential displacement noise. A rearrangement and simplification of the optics on this optical bench reduced this source of scattering to a level where it no longer limits the sensitivity of GEO 600. The main aim here was to move any scattering surfaces away from the beam waist where the angle of acceptance is very large and to allow for the use of only high quality optics.

2.2. Noise projections

An essential aspect of the commissioning work is the projection of various technical noise sources to the detector output. This can yield valuable information about which noise sources are currently limiting the sensitivity of the detector and therefore, where work should be focused. The noise projections carried out at GEO 600 are mainly done by using measured transfer functions from some point in a particular subsystem to the detector outputs. For example, we can inject white noise into a point after the error-point of the Michelson differential-length-control servo and measure the transfer function from the feedback point to the error-point. We can then measure the noise at the feedback point during normal lock of the Michelson and project it to the detector output using the measured transfer function. (This assumes that the transfer function is still valid for the time that we want to project.) The projected noise can then be converted to apparent strain so that it can be compared directly to the calibrated strain sensitivity of the detector.

Figure 5 shows a snap-shot of various technical noise sources projected to apparent strain. Feedback noise is shown projected for the signal-recycling and Michelson longitudinal length-control servos. In some cases where a direct measurement is difficult a modelled noise source is used to help give an impression of whether we have suitably explained the noise floor we see. For example, the behaviour of the noise level versus power on the output photodiode was fit with a model: a dark noise that did not vary with power, and a shot noise that varied with the square-root of power. This was consistent with the measured noise at high frequencies, especially in the Q quadrature. This model is shown as the dotted line in figure 5.

Also shown in figure 5 is the uncorrelated sum of all the projected noises. It is clear that the limiting noise source at all frequencies is not included in this figure. Further investigations are required to identify the limiting noise source at this time. For example, not included in the current picture is the projection of noise present around the rf signal used to produce the Michelson modulation control sidebands; this could couple to the main detector output as both amplitude and phase noise.

3. Reconstructing the apparent strain signal

GEO 600 uses a time-domain calibration technique with a latency of a few seconds to perform on-line calibration of the two demodulated detector outputs.

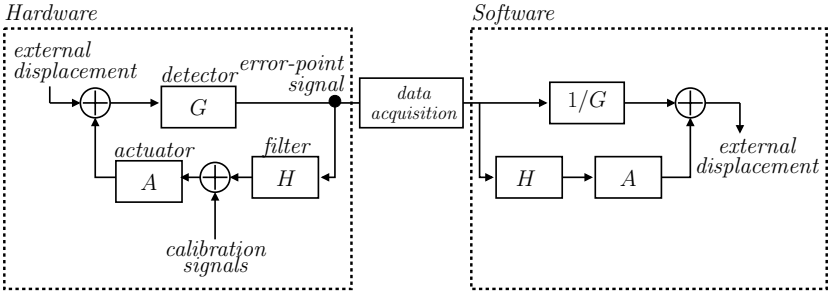

Figure 4. A schematic representation of the principles involved in calibrating the dual-recycled GEO 600 in the time domain. The transfer function from differential arm-length change to detector output, which includes the optical cavity response and the Michelson differential-length-control servo response, is inverted in software and applied to the recorded signals to recover the apparent strain of the detector.

By continuously injecting a set of periodic signals at different frequencies into the differential-length-control actuators of the Michelson differential servo, the response of the detector to differential arm-length changes, and hence strain, can be monitored quasi-continuously. The injected calibration lines are measured at both the injection point and the two detector outputs, $P(t)$ and $Q(t)$, once per second. We then form the complex ratios of calibration lines in P and Q to the injected lines and fit these spot transfer function measurements to a parametrized model of the detector transfer function from differential arm-length change to P and Q.

These 1 Hz estimates of the detector response are then used to create time-domain filters that, when applied to $P(t)$ and $Q(t)$, give two estimates, $h_P(t)$ and $h_Q(t)$, of the strain sensitivity of the detector. Figure 4 shows a schematic of this process for only one output quadrature: the calibration of the other quadrature is done in a similar way. The method and its application is discussed in detail in [15–18].

3.1. Calibration of both demodulated output signals

At the time of the S3 science run, only the P quadrature was calibrated to strain sensitivity using the time-domain method described above. During the first half of 2004, the calibration method was extended to include calibration of the other (Q) demodulated output quadrature. To achieve this, the model of the optical transfer function had to be extended and the code put in place to produce the appropriate time-domain filters.

Having $h_Q(t)$ as well as $h_P(t)$ became a very useful diagnostic for commissioning work. Figure 6 shows the sensitivity improvement of GEO 600 as measured by the h_Q calibrated output. Here we see that some of the commissioning steps produced even larger improvements in the Q quadrature than in P (see figure 3), particularly at higher frequencies, above the signal-recycling resonance frequency.

Since, at the end, we want to combine $h_Q(t)$ and $h_P(t)$ to give a single, optimal $h_{\rm opt}(t)$ signal, more and more effort was put into reducing the noise in the Q quadrature, particularly as the sensitivity of any combined $h_{\rm opt}(t)$ would be limited by the noise in this quadrature at high frequencies. To aid this effort, the noise projection scheme that previously concentrated only on the P quadrature was extended to include the Q quadrature. Examples of various technical noise sources present in the subsystems of GEO 600 are shown in figure 7 projected to apparent strain.

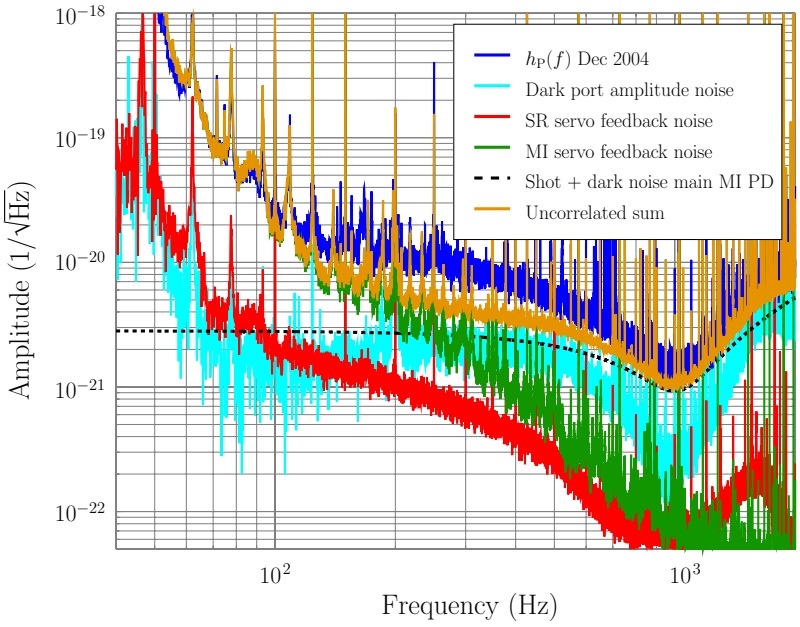

Figure 5. Various measured technical noises of GEO 600 projected to the calibrated *P* quadrature output and displayed as apparent strain; the sensitivity spectrum for the calibrated *P* quadrature at the time of the projections is shown for reference.

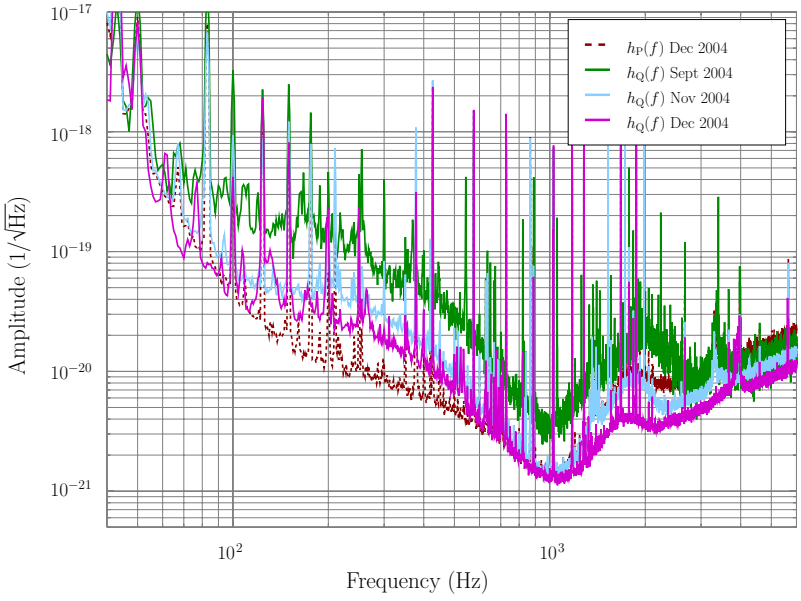

Figure 6. The sensitivity of the *Q* quadrature of GEO 600 at various epochs between September and December 2004. Each increase in sensitivity can be associated by date with those improvements discussed in relation to the *P* quadrature sensitivity.

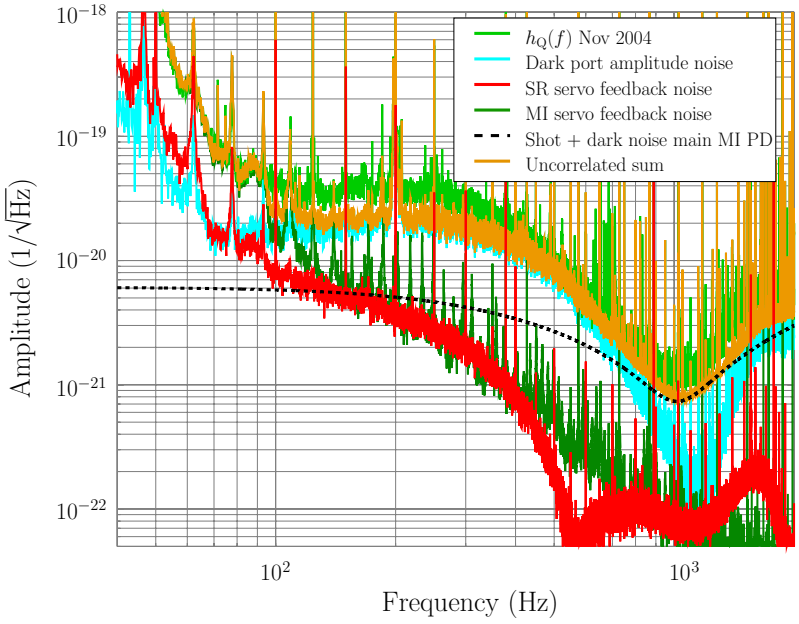

Figure 7. Various measured technical noises of GEO 600 projected to the Q quadrature output and displayed as apparent strain; the sensitivity spectrum for the Q quadrature at the time of the projections is shown for reference.

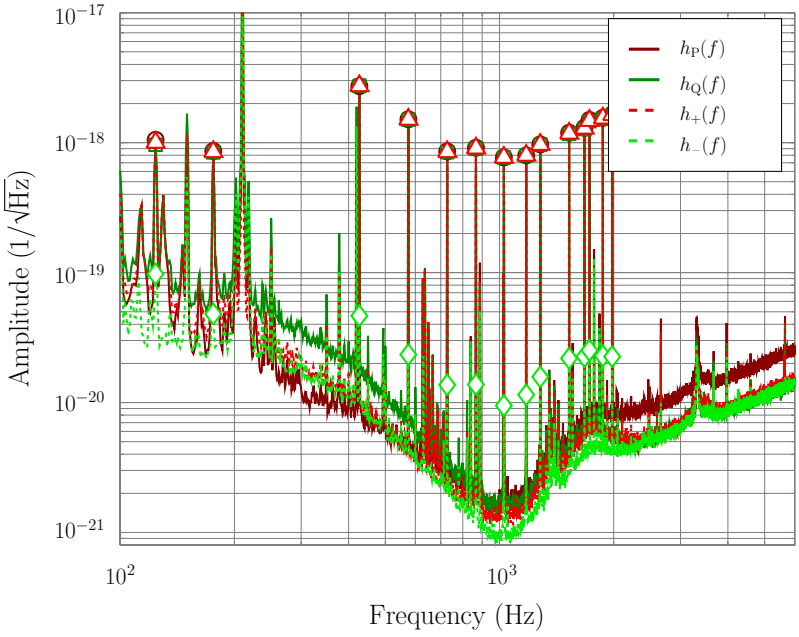

Figure 8. Snap-shot spectra of two possible combinations of $h_P(t)$ and $h_Q(t)$; one (h_+) where we expect to see the gravitational wave signal (exemplified by the calibration lines) preserved, the other (h_-) where we expect (almost) no gravitational wave signal to be present.

3.2. Combining two calibrated strain signals

After the calibration of the Q quadrature was fully in place and tested over a period of time, work on combining the two $h(t)$ signals was started. Initially some simple combining methods were explored to get an impression of what might be achieved with more sophisticated algorithms.

We start from the fact that both the calibrated outputs, $h_P(t)$ and $h_Q(t)$, contain the same underlying gravitational wave signal to within the accuracy of the calibration process. In other words,

$$h_P(t) = h(t) + n_P, \tag{1}$$

$$h_Q(t) = h(t) + n_Q. \tag{2}$$

It is most likely the case that some of the noise (n_P and n_Q) in the two quadratures is the same, but in this case it would be indistinguishable from the signal (for example, differential displacement noise from seismic activity).

Based on the above formulation, one method that was tried was to make the mean of the two $h(t)$ signals in the time domain, with the hope that we get a better signal-to-noise ratio (at least at some frequencies) than either of the calibrated P and Q signals. We can also form the difference of the two $h(t)$ signals such that we get two new signals, $h_+(t)$ and $h_-(t)$, where

$$h_+(t) = \tfrac{1}{2}(h_P(t) + h_Q(t)), \tag{3}$$

$$h_-(t) = \tfrac{1}{2}(h_P(t) - h_Q(t)). \tag{4}$$

In the signal h_+ we expect the underlying gravitational wave signal to be preserved, whereas in the h_- signal we would expect no gravitational wave signal, at least to a level consistent with the calibration accuracy and the signal-to-noise ratio. Figure 8 shows snapshot spectra of these two combined $h(t)$ signals, together with the original calibrated $h(t)$ signals for comparison. We can see that for the h_+ signal, the calibration lines match well with $h_P(t)$ and $h_Q(t)$, whereas the calibration lines in the h_- signal are reduced to a level consistent with the accuracy of the calibration process (typically around 5%). We can also see that the h_+ signal has (at least at high frequencies) better signal-to-noise ratio than either $h_P(t)$ or $h_Q(t)$. However, at lower frequencies, this simple method means that we lose some sensitivity. A more sophisticated frequency-dependent method is clearly needed to get the best sensitivity at all frequencies across the detection band.

4. Summary and future commissioning steps

Continued reduction of technical noise sources will persist in playing the central role in commissioning of GEO 600, especially as we get closer and closer to design sensitivity. However, a small number of significant hardware changes remain to be implemented to allow design sensitivity to be reached. In particular, the injected laser power will be increased to 10 W which together with a change of the power-recycling mirror will give an intracavity power of the interferometer of 10 kW. This level of circulating power is needed if we are to reach the design shot-noise limited sensitivity at high frequencies.

To help combat the various technical noises, all output optics that direct the main output beam to the high-power photodiode have been installed within the vacuum system. At the current time, the vacuum tank that houses the high-power photodiode and associated beam steering mirrors is isolated from the main ultra-high-vacuum system and is not evacuated since

we are not currently limited by any acoustic or refractive noise in this part of the beam path. When this state changes, the tank will be pumped down.

Once all the hardware changes are done and all technical noise sources are removed as far as possible, the final small increase in sensitivity may well be gained by producing an optimal combination of the two calibrated outputs, $h_P(t)$ and $h_Q(t)$. To achieve this, a method needs to be developed that, in a frequency-dependent way, can combine these two signals in the time domain, thus maintaining the on-line production of a calibrated strain sensitivity which has proved very useful in the commissioning of the dual-recycled GEO 600 and for subsequent analysis, and which may become increasingly important as more and more of the astrophysical searches start to run on-line.

References

[1] Sigg D *et al* 2004 Commissioning of LIGO detectors *Class. Quantum Grav.* **21** S409–15
[2] Acernese F *et al* 2004 Status of VIRGO *Class. Quantum Grav.* **21** S385–94
[3] Takahashi R (the TAMA Collaboration) 2004 Status of TAMA300 *Class. Quantum Grav.* **21** S403–8
[4] Willke B *et al* 2004 Status of GEO 600 *Class. Quantum Grav.* **21** S417–23
[5] Heng I S, Daw E, Giaime J, Hamilton W O, Mchugh M P and Johnson W W 2002 Allegro: noise performance and the ongoing search for gravitational waves *Class. Quantum Grav.* **19** 1889–95
[6] Zendri J-P *et al* 2002 Status report and near future prospects for the gravitational wave detector AURIGA *Class. Quantum Grav.* **19** 1925–33
[7] Astone P (ROG Collaboration) 2004 Seven years of data taking and analysis of data from the Explorer and Nautilus gravitational wave detectors *Class. Quantum Grav.* **21** S1585–94
[8] Heinzel G *et al* 2002 Dual recycling for GEO 600 *Class. Quantum Grav.* **19** 1547–53
[9] Grote H, Freise A, Malec M, Heinzel G, Willke B, Lück H, Strain K A, Hough J and Danzmann K 2004 Dual recycling for GEO 600 *Class. Quantum Grav.* **21** S473–80
[10] Zawischa I, Brendel M, Danzmann K, Fallnich C, Heurs M, Nagano S, Quetschke V, Welling H and Willke B 2002 The GEO 600 laser system *Class. Quantum Grav.* **19** 1775–81
[11] Goßler S *et al* 2003 Mode-cleaning and injection optics of the gravitational wave detector, GEO 600 *Rev. Sci. Instrum.* **74** 3787
[12] Plissi M, Torrie C I, Housman M, Robertson N A, Strain K A, Ward H, Lück H and Hough J 2000 GEO 600 triple pendulum suspension system: seismic isolation and control *Rev. Sci. Instrum.* **71** 2539–45
[13] Goßler S, Cagnoli G, Crooks D R M, Lück H, Rowan S, Smith J R, Strain K A, Hough J and Danzmann K 2004 Damping and tuning of the fibre violin modes in monolithic silica suspensions *Class. Quantum Grav.* **21** S923–33
[14] Smith J R *et al* 2004 Commissioning, characterization, and operation of the dual-recycled GEO 600 *Class. Quantum Grav.* **21** S1737–45
[15] Hewitson M, Grote H, Heinzel G, Strain K A, Ward H and Weiland U 2003 Calibration of the power-recycled gravitational wave detector, GEO600 *Rev. Sci. Instrum.* **74** 4184–90
[16] Hewitson M, Grote H, Heinzel G, Strain K A, Ward H and Weiland U 2003 Calibration of GEO 600 for the S1 science run *Class. Quantum Grav.* **20** S885–93
[17] Hewitson M, Heinzel G, Smith J R, Strain K A and Ward H 2004 Principles of calibrating the dual-recycled GEO 600 *Rev. Sci. Instrum.* **75** 4702–9
[18] Hewitson M *et al* 2004 Calibration of the dual-recycled GEO 600 detector for the S3 science run *Class. Quantum Grav.* **21** S1711–22